Smoking promotes colorectal cancer via the CKAP2L/AREG axis

SHASHA WU[1-3*], FEIXIANG WU[3,4*], XIAOQING LI[1], ZHIHANG JIANG[1], FUQIANG LIU[1,3,5] and ZHENG JIANG[1]

[1]Department of Gastroenterology, The First Affiliated Hospital of Chongqing Medical University, Chongqing 400016, P.R. China; [2]Department of Gastroenterology, The Third Hospital of Mianyang, Sichuan Mental Health Center, Mianyang, Sichuan 621000, P.R. China; [3]Chongqing Key Laboratory of Molecular Oncology and Epigenetics, The First Affiliated Hospital of Chongqing Medical University, Chongqing 400016, P.R. China; [4]Department of Urology, The Third Hospital of Mianyang, Sichuan Mental Health Center, Mianyang, Sichuan 621000, P.R. China; [5]Department of Gastroenterology, The People's Hospital of Jianyang City, Jianyang, Sichuan 641400, P.R. China

Received September 17, 2025; Accepted February 24, 2026

DOI: 10.3892/ijo.2026.5872

Abstract. The link between smoking and colorectal cancer (CRC) is well-established; however, further research is needed to fully understand the specific effects of tobacco on the development of this type of cancer. The aim of the present study was to investigate the relationship between smoking and CRC, as well as to identify key genes involved in smoking-enhanced CRC progression. To confirm the association between smoking and CRC, analyses of clinical data from the National Health and Nutrition Examination Survey database and genome-wide association studies data were integrated. In addition, RNA sequencing (RNA-seq) was conducted on HCT116 cells treated with cigarette smoke extract to identify genes related to smoking. To evaluate the malignant phenotypes of CRC cells and potential molecular mechanisms by which key genes promote smoking-enhanced CRC, a series of cell and animal experiments were performed. The positive association between smoking and CRC was confirmed by both the cross-sectional study and Mendelian randomization analyses. Furthermore, after treatment of CRC cells with cigarette smoke extract, cell proliferation, migration and invasion were enhanced. Subsequently, cytoskeleton-associated protein 2-like (CKAP2L) was filtered out by bioinformatics analysis, indicating its involvement in smoking-enhanced CRC. After suppressing CKAP2L, the results revealed that cell proliferation was inhibited, and the cell cycle was arrested at S and G_2/M phases. Moreover, cell migration and invasion were suppressed after suppressing CKAP2L expression. Further RNA-seq analysis suggested that CKAP2L promotes the expression of amphiregulin (AREG). Subsequently, the suppression of AREG resulted in a reduction in the CKAP2L-promoted proliferation and migration of CRC cells. The results of a chromatin immunoprecipitation assay further confirmed that signal transducer and activator of transcription 3 (STAT3) regulated the transcriptional level of AREG by binding to its promoter. In addition, CKAP2L increased the phosphorylation of STAT3, which subsequently activated the AREG/EGFR pathway, leading to the progression of CRC. In conclusion, the present study demonstrated that smoking may promote CRC progression through the CKAP2L/AREG axis.

Correspondence to: Professor Zheng Jiang, Department of Gastroenterology, The First Affiliated Hospital of Chongqing Medical University, 1 Youyi Road, Yuzhong, Chongqing 400016, P.R. China
E-mail: jiangz1753@hospital.cqmu.edu.cn

*Contributed equally

Abbreviations: CRC, colorectal cancer; MR, Mendelian randomization; ChIP, chromatin immunoprecipitation; CKAP2L, cytoskeleton-associated protein 2-like; AREG, amphiregulin; STAT3, signal transducer and activator of transcription 3; GWAS, genome-wide association studies; IV, instrumental variable; EGFR, epidermal growth factor receptor; SNP, single-nucleotide polymorphism; IVW, inverse-variance weighted; FE, fixed effect; MRE, multiplicative random effect; RNA-seq, RNA sequencing; scRNA-seq, single-cell RNA-seq; DEG, differentially expressed gene; CSE, cigarette smoke extract; CCK8, cell Counting Kit 8; shRNA, short hairpin RNA; OE, overexpression; siRNA, small interfering RNA; ELISA, enzyme-linked immunosorbent assay; EdU, 5-ethynyl-2'-deoxyuridine; EMT, epithelial-mesenchymal transition

Key words: smoking, CRC, CKAP2L, AREG, National Health and Nutrition Examination Survey, Mendelian randomization

Introduction

Among all risk factors for cancer, smoking is the most important and controllable one; notably, it is frequently observed that smoking cessation can result in a reduction of this risk (1,2). Cigarette smoke has been reported to contain carcinogenic compounds, including nitrosamines, polycyclic aromatic hydrocarbons and volatile organic compounds, which lead to mutations in critical cancer genes, such as KRAS and TP53 (3,4). Colorectal cancer (CRC) is the third most prevalent type of cancer worldwide (5), and globally, smoking is a common risk factor for CRC, contributing to ~13.3% of CRC cases (6). Previous studies have confirmed the association between smoking and CRC by performing correlation and Mendelian randomization (MR) analyses (7,8). Animal experiments have also revealed that cigarette smoke increases the incidence of CRC and promotes cell proliferation by inducing

gut microbiota dysbiosis (9). However, there is still a lack of research on critical genes that regulate the progression of smoking-associated CRC.

The National Health and Nutrition Examination Survey (NHANES) database (https://wwwn.cdc.gov/nchs/nhanes/) contains abundant survey data and has been widely used in observation studies (10-13). MR analysis is a robust method for causality assessment (14); notably, genome-wide association studies (GWAS) provide ideal instrumental variables (IVs) and have been widely used in MR analyses (11). In the present study, observational studies and MR analyses were employed to systematically assess the link between different smoking characteristics and CRC.

Bioinformatics analyses have been widely used to identify critical molecules of diseases (15). In the current study, the critical genes implicated in the smoking-enhanced progression of CRC were identified by integrative bioinformatics analyses. By overlapping CRC-related genes and smoking-related genes, the current study aimed to filter out the key genes involved in smoking-enhanced CRC. Cytoskeleton-associated protein 2-like (CKAP2L) is a component of the cell centrosome, which serves a critical role in spindle formation (16,17). As reported in bladder cancer, esophageal squamous cell carcinoma and lung cancer, CKAP2L mediates the cell cycle and promotes the progression and dissemination of tumors (18-20). A recent study reported that regulatory factor X5-regulated CKAP2L can stimulate the proliferation, migration and invasion of CRC cells (21). Amphiregulin (AREG) is a ligand of epidermal growth factor receptor (EGFR) and promotes cancer progression via activating EGFR signaling (22). The present study aimed to identify the key genes involved in smoking-enhanced CRC and reveal the potential mechanisms by which key genes promote the progression of CRC.

Materials and methods

Investigation of the association between smoking and CRC. The clinical association between smoking features (smoking status, cotinine and age started smoking) and CRC was analyzed based on 1999-2018 NHANES survey datasets (https://wwwn.cdc.gov/nchs/nhanes/default.aspx). After excluding participants under the age of 20 years, those who were pregnant or those with missing variables, 37,091 participants were finally included in the cross-sectional study.

Smoking status was defined by two questions: 'Smoked at least 100 cigarettes in life?' and 'Do you now smoke cigarettes?' Cotinine is a major metabolite of nicotine and can be used as a marker for smokers and an indicator of secondhand smoke exposure. Due to the recall bias in self-reported secondhand smoke exposure (exposure source or duration), for individuals who have never smoked, a serum cotinine level of ≥0.015 ng/ml (lower detection limit) was considered secondhand smoke exposure according to previous studies (23,24). The participants were subsequently divided into four different smoking statuses: No smoking, past smoking, current smoking and secondhand smoking. Previous studies have reported that 3 ng/ml is a recommended cut-off point for cotinine levels (25-27), whereas ≥10 ng/ml is always observed in active smokers (28). Therefore, serum cotinine levels were divided into <0.015, 0.015-3, 3-10 and ≥10 ng/ml. Age at which individuals started smoking cigarettes regularly was divided into three groups: Never regularly smoked, <20 and ≥20 years. CRC was defined according to the first reported cancer type. The following covariates were adjusted in the subsequent analyses: Age, sex, ethnicity, marital status, education, ratio of family income to poverty, body mass index and alcohol consumption. Those who had consumed ≥12 alcohol drinks/1 year or lifetime were defined as having alcohol consumption. The baseline characteristics revealed the differences between the CRC and non-CRC groups (Table SI). Continuous data were compared using survey-weighted linear regression, whereas categorical data were compared using survey-weighted χ^2 test.

Due to the complex sampling design of the NHANES survey, sample weights, strata and primary sampling units were considered in all analyses. The association between CRC and smoking was assessed by three logistic regression models: Model 1, non-adjusted; model 2, adjusted for age, sex and ethnicity [these characteristics show notable differences in smoking habits and CRC occurrence (29-31)]; and model 3, fully adjusted. All analyses were performed using EmpowerStats software (version 4.1; X&Y Solutions, Inc.). $P<0.05$ was considered to indicate a statistically significant difference.

The causality of smoking and CRC was measured by two-sample MR analyses. GWAS data for CRC (n=293,646) were downloaded from FinnGen (https://www.finngen.fi/en/access_results). Pooled GWAS data for age of initiation of regular smoking (n=341,427), cigarettes per day (n=337,334), smoking cessation (n=547,219) and smoking initiation (n=1,232,091) were extracted from a meta-analysis (32). GWAS data for pack years of adult smoking as a proportion of life span exposed to smoking (n=142,387) were downloaded from the IEU database (https://gwas.mrcieu.ac.uk/datasets/ukb-b-7460/). All participants in these GWAS datasets were European and the details of the GWAS data are listed in Table SII.

The identification of IVs conformed to three assumptions: Relevance, independence and exclusion restriction. Single-nucleotide polymorphisms (SNPs) with $P<5x10^{-8}$ and a linkage disequilibrium of $r^2<0.001$ within 10,000-kb windows were selected as IVs for smoking. Palindromic SNPs were harmonized. Finally, 13 SNPs were identified as IVs for pack years of adult smoking. R^2 was calculated to reveal the proportion of exposure variation explained by SNPs. The F-statistic was calculated to assess the strength of the association between the SNP and exposure. SNPs with F≥10 were considered as strong genetic instruments and were included in the subsequent analysis.

The inverse-variance weighted (IVW), weighted median, simple mode and weighted mode methods in 'TwoSampleMR' package (version 0.6.19; https://github.com/MRCIEU/TwoSampleMR) in R software 4.2.2 (https://www.r-project.org/) were used for MR analysis, in which the IVW method was the main method. Selection of the IVW fixed effect (IVW_FE) or IVW multiplicative random effect (IVW_MRE) method was dependent on heterogeneity, which was evaluated by Cochran's Q test. If heterogeneity existed, IVW_MRE was the main method. MR-Egger intercept analysis was performed to assess directional pleiotropy. MR-PRESSO, funnel plot and leave-one-out analyses

were conducted to detect outliers. Outliers were excluded by MR-PRESSO and the remaining IVs were included in the final MR analysis. MR analyses were conducted with the 'TwoSampleMR' package in R software 4.2.2 (https://www.r-project.org/). Bonferroni-corrected P<0.01 (0.05/5=0.01) was defined as the significance criterion for MR estimation, whereas P<0.05 was considered to indicate a statistically significant difference in other tests. Both cross-sectional and MR analyses were supervised by a trained statistician and a bioinformatician.

Bioinformatics analyses. To identify hub genes of CRC, The Cancer Genome Atlas (TCGA) datasets (https://portal.gdc.cancer.gov/) for CRC (colon adenocarcinoma and rectum adenocarcinoma), including 650 tumors and 51 healthy controls, were downloaded. In addition, bulk RNA sequencing [RNA-seq; GSE200130 (33), https://www.ncbi.nlm.nih.gov/geo/query/acc.cgi?acc=GSE200130; 12 tumor samples and 13 healthy control samples] and single-cell RNA-seq [scRNA-seq; GSE200997 (34), https://www.ncbi.nlm.nih.gov/geo/query/acc.cgi?acc=GSE200997; 16 tumors and 7 adjacent normal tissues] datasets were downloaded from the Gene Expression Omnibus database. These datasets were used in the bioinformatics analysis.

Differentially expressed genes (DEGs) in epithelial cells between CRC and normal samples were filtered out based on scRNA-seq, using 'Seurat' (v5; https://satijalab.org/seurat/) and 'harmony' (release 0.1; https://github.com/immunogenomics/harmony) packages. The upregulated DEGs were identified with $\log_2$FoldChange (FC)>0.585 and adjusted P<0.05. For GSE200130 and TCGA datasets, upregulated DEGs with logFC>1 and adjusted P<0.05 were identified with the 'DESeq2' (35) package (version 1.44.0; https://www.bioconductor.org/packages/release/bioc/html/DESeq2.html). Moreover, weighted gene co-expression network analysis (WGCNA) was performed on TCGA datasets to further select genes positively linked to CRC using the 'WGCNA' (36) package (version 1.73). By overlapping the aforementioned upregulated DEGs and genes positively related to CRC, the CRC-related genes were identified.

The key genes involved in smoking-enhanced CRC were selected by overlapping the CRC-related genes and smoking-related genes. All analyses were conducted using R software 4.2.2.

Cell lines and inhibitor. To investigate the hypothesis that key genes promote the progression of smoking-enhanced CRC in different subtypes of CRC, and ensure the reliability and universality of the research results, four human CRC cell lines were used. The human CRC cell lines SW480, Caco-2, HCT116 and RKO, the mouse CRC cell line CT26, the human normal colonic cell line NCM460 and 293T cells were purchased from Ubigene Biosciences. All cells were cultured in DMEM (Gibco; Thermo Fisher Scientific, Inc.) supplemented with 10% fetal bovine serum (FBS; Pricella; Elabscience Bionovation Inc.) at 37˚C and 5% CO_2. The signal transducer and activator of transcription 3 (STAT3) phosphorylation inhibitor Stattic (cat. no. HY-13818; MedChemExpress) was dissolved in DMSO for cell culture. HCT116 cells were cultured with Stattic at a final concentration of 2 μM for 24 h at 37˚C and 5% CO_2.

Construction of cell models treated with CSE. According to previous studies (18,37,38), CSE was freshly prepared and used to treat cells within 30 min. The details of CSE preparation and usage were published in our previous study (18). Briefly, a cigarette (brand: Hongtashan) was burned for ~5 min and its mainstream smoke was absorbed in 10 ml DMEM. After filtering through a 0.22-μm filter, the solution was regarded as a 100% CSE solution. Upon preparation, CSE was diluted to the concentrations of 0.0625, 0.125, 0.25, 0.5, 1, 2 and 4% CSE using DMEM and was then used to treat the CRC cell lines at 37˚C for 4 days, including Caco-2, RKO and HCT116 cells. The cells were then incubated with the Cell Counting Kit 8 (CCK8; cat. no. BS350C; Biosharp Life Sciences) reagent for 1 h at 37˚C to evaluate the impact of varying concentrations of CSE on cell viability. Subsequently, according to the results of short-time CSE treatment, CRC cells (RKO and HCT116) were cultured with 0.125 and 0.25% CSE for 2 months to reveal the influence of chronic smoke exposure on proliferation, migration and invasion.

Cell transfection and transduction. All plasmids and small interfering RNA (siRNA) were synthetized by Beijing Tsingke Biotech Co., Ltd., and the details of the short hairpin RNA (shRNA; Beijing Tsingke Biotech Co., Ltd.) and siRNA sequences are shown in Table SIII. A total of four shCKAP2L plasmids were synthesized and used, and the shRNA-negative control (non-targeting) plasmid was set as the control. For the CKAP2L overexpression (CKAP2L-OE) plasmid, the corresponding empty plasmid without the CKAP2L gene insert was used as the control. First, all of the OE and shRNA plasmids (PLVX-puro; Beijing Tsingke Biotech Co., Ltd.) were transfected into 293T cells to generate lentiviral particles, and these lentiviral particles were then transduced into CRC cells. Briefly, to generate lentiviral particles, 293T cells were seeded in a 10-cm culture dish and incubated overnight until the cell density reached 70-80%. A total of 10 μg plasmids (5 μg target plasmid, 3.75 μg psPAX2 and 1.25 μg pMD2.G) were co-transfected into 293T cells with 20 μl Lipofectamine® 2000 (cat. no. 11668027; Invitrogen; Thermo Fisher Scientific, Inc.). The viruses were then collected 48 and 72 h after transfection, and were mixed together for cell transduction according to previous studies (39-41) in CRC cell lines (RKO, Caco-2, HCT116 and CT26). Cells were transduced with 500 μl collected supernatant containing lentiviral particles for 18 h at 37˚C and 5% CO_2. A total of 48 h post-transduction, stable cells were filtered with puromycin (selection, 2 μg/ml; maintenance, 1 μg/ml).

For siAREG and siRNA-negative control transfection, HCT116 cells were pre-plated in a 6-well plate and incubated overnight until they reached 70-80% confluence. Subsequently, 50 μM siRNA was transfected into the cells with 5 μl Lipofectamine 2000. After incubation at 37˚C for 4-6 h, the transfection complex was replaced with fresh culture medium. A total of 24 h post-transfection, the mRNA expression was measured, and after 48 h, the protein expression, and cell migration and proliferation were detected.

Reverse transcription-quantitative PCR (RT-qPCR). RNA was extracted from cells using TRIzol® reagent (cat. no. 15596026; Invitrogen; Thermo Fisher Scientific, Inc.)

according to the manufacturer's instructions. RNA was then reverse transcribed into cDNA using the qPCR RT Master Mix (cat. no. FSQ-201; Toyobo Co., Ltd.) (RNA: 1 μg; 5X RT Master Mix: 2 μl; nuclease-free water: ≤10 μl; steps: 37˚C for 15 min, 50˚C for 5 min, 98˚C for 5 min and maintained at 4˚C). qPCR was performed using the SYBR® Green Realtime PCR Master Mix (cat. no. QPK-201; Toyobo Co., Ltd.) according to the manufacturer's instructions [nuclease-free water: 3.2 μl; forward primer (10 μM): 0.4 μl; reverse primer (10 μM): 0.4 μl; cDNA: 1 μl; SYBR Green Realtime PCR Master Mix: 5 μl; steps: 95˚C for 60 sec, followed by 40 cycles at 95˚C for 5 sec, 60˚C for 15 sec and 72˚C for 45 sec, and melting curve analysis]. The mRNA expression levels were calculated using the $2^{-\Delta\Delta Cq}$ method (42). The primer sequences are listed in Table SIV.

RNA-seq. HCT116 cells were treated with CSE for 8 weeks and underwent RNA extraction. RKO cells stably transduced with shCKAP2L #1 and HCT116 cells stably transduced with CKAP2L-OE also underwent RNA extraction using TRIzol reagent, according to the manufacturer's instructions. Subsequently, the extracted RNA was sent to Sangon Biotech Co., Ltd. for further processing and RNA sequencing. The integrity of the RNA and DNA contamination were detected by agarose gel electrophoresis on 1% gels. Based on the Illumina HiSeq 2500 platform (Illumina, Inc.), 150-bp paired-end sequencing (direction: Forward and reverse) was conducted using the HiSeq Rapid SBS Kit v2 (cat. no. FC-402-4022; Illumina, Inc.). The loading concentration of the final library was 6 pM. The sequencing data were analyzed using the 'DESeq2' package and were visualized in volcano plots. For self-conducted RNA-seq, the upregulated genes (logFC>0.263 and adjusted P<0.05) in the CSE-treated group were identified as smoking-related genes using the 'DESeq2' package.

Western blotting. RIPA buffer (cat. no. P0013B; Beyotime Biotechnology) was employed to extract total proteins from cells and a BCA kit (cat. no. P0010S; Beyotime Biotechnology) was used to detect protein concentration. A total of 40 μg protein/lane was separated by SDS-PAGE (cat. no. P0012AC; Beyotime Biotechnology) on 10-12% gels, and the proteins were then transferred to PVDF membranes. Subsequently, the membranes were incubated in 5% skim milk at room temperature for 1 h, and the washed membranes were immersed in primary antibodies (Table SV) at 4˚C overnight. β-actin was used as the loading control. After incubation with the corresponding secondary antibodies (HRP-conjugated Goat Anti-Rabbit IgG, 1:5,000, cat. no. SA00001-2, Proteintech Group, Inc.; HRP-conjugated Goat Anti-Mouse IgG, 1:5,000, cat. no. SA00001-1, Proteintech Group, Inc.) at room temperature for 1 h, an ECL kit (cat. no. P0018S; Beyotime Biotechnology) and Fusion software (Fusion FX; Vilber Lourmat) were employed to measure protein signals. Subsequently, the semi-quantification of images was performed by ImageJ (version 1.54 g; National Institutes of Health).

Enzyme-linked immunosorbent assay (ELISA). HCT116 cells were maintained with complete medium supplemented with 2% FBS for 24 h and the medium was collected. The concentration of secreted AREG in the culture medium was then measured using the Human AREG ELISA Kit (cat. no. EK0304; Wuhan Boster Biological Technology, Ltd.) according to the manufacturer's instructions. Briefly, samples were added to the plate that was precoated with antibody and were incubated at 37˚C for 90 min. After discarding the liquid, the biotin-labeled anti-human AREG antibody was added to the plate and incubated at 37˚C for 60 min. After washing the plate, ABC solution was added and incubated at 37˚C for 30 min. Finally, the plate was washed again and TMB solution was added for color generation. The OD value at 450 nm was detected using a microplate reader (Tecan Group, Ltd.).

Chromatin immunoprecipitation (ChIP). The transcriptional regulatory effect of STAT3 on AREG was evaluated using the Cistrome Data Browser (http://cistrome.org/db/) (43) and JASPAR database (https://jaspar.elixir.no/) (44). This effect was confirmed using a ChIP assay kit (cat. no. P2080S; Beyotime Biotechnology), which was performed according to the manufacturer's instructions. Briefly, RKO cells were cultured in a 10-cm culture dish. Cross-linking was carried out by incubation with 1% formaldehyde at 37˚C for 10 min, after which, SDS lysis buffer was added to the cells and incubated on ice for 10 min. Subsequently, chromatin was fragmented to 400-800 bp using ultrasonication at 0˚C (20 kHz; power: 38W; ultrasonic treatment for 10 sec, pause for 10 sec; 20 cycles.). After fragmentation, the lysate was incubated with 2 μg anti-STAT3 (cat. no. 60199-1-Ig; Proteintech Group, Inc.) or 2 μg IgG (cat. no. 30000-0-AP; Proteintech Group, Inc.) at 4˚C overnight. Subsequently, 80 μl protein A/G beads (MedChemExpress) were incubated with the aforementioned antibody and lysate complex at 4˚C for 1 h and chromatin was eluted with elution buffer (1% SDS and 0.1 M $NaHCO_3$) and was incubated at 65˚C for 4 h to reverse crosslinking. The purified DNA was subjected to qPCR analysis as aforementioned.

Cell proliferation assays. The CCK8 reagent (cat. no. BS350C; Biosharp Life Sciences) was employed to measure cell proliferation. Transduced and transfected cells (RKO, Caco-2 and HCT116) were cultured at a density of 2,000 cells/well for 0, 24, 48 and 72 h. Subsequently, 10 μl CCK8 reagent was added to 100 μl medium and incubated with the cells for 1-2 h. Subsequently, a microplate reader (Tecan Group, Ltd.) was employed to detect the absorbance at 450 nm.

The 5-ethynyl-2'-deoxyuridine (EdU) assay was also conducted to assess cell proliferation. EdU reagent was added to medium and incubated with the CSE-treated or transduced RKO, Caco-2 and HCT116 cells (60-70% confluence) for 2 h. Subsequently, the cells were incubated with 4% paraformaldehyde at room temperature for 15 min, treated with Triton X-100 at room temperature for 15 min, and stained with an EdU kit (cat. no. BL917A; Biosharp Life Sciences) and Hoechst. Finally, images were obtained under a fluorescence microscope (Leica Microsystems GmbH).

A colony formation assay was also conducted using 6-well plates. In each well, 1,500 transfected cells (RKO, Caco-2 and HCT116) were seeded and cultured for 14 days. Subsequently, the colonies were fixed with 4% paraformaldehyde at room temperature for 15 min and stained with 0.1% crystal violet

at room temperature for 15 min, images were captured and the colonies consisting of >50 cells were counted under a light microscope (Leica Microsystems GmbH).

Cell cycle analysis. Flow cytometry was employed to detect cell cycle progression. Transduced RKO, Caco-2 and HCT116 cells at 80% confluence were harvested and fixed with 75% ethanol for >24 h at 4˚C. The fixed cells were then stained with PI/RNase Staining Buffer (cat. no. 550825; BD Biosciences) at room temperature for 15 min, and immediately submitted to cell cycle detection by flow cytometry using a CytoFLEX flow cytometer (Beckman Coulter, Inc.) and CytExpert software (Version 2.6; Beckman Coulter, Inc.).

Assessment of cell migration and invasion. Transwell assay is a classic method used to assess cell migration and invasion. To measure migration, $5x10^4$ cells (RKO, Caco-2 and HCT116) were resuspended in 200 μl serum-free medium and seeded in the upper chamber of a Transwell plate (cat. no. 3422; Corning, Inc.). Subsequently, complete medium was added to the lower chamber. After 48 h at 37˚C, the migrated cells were incubated with 4% paraformaldehyde at room temperature for 15 min and 0.1% crystal violet at room temperature for 15 min, successively. Under a light microscope, images of migrated cells were captured. For invasion, after pre-coating the Transwell plate with Matrigel (cat. no. 356234; Corning, Inc.), $5x10^4$ cells were resuspended in 100 μl serum-free medium and seeded in the upper chamber. The subsequent steps were identical to those performed in the migration assay.

The wound healing assay is also a common method used to measure cell migration. Briefly, RKO and HCT116 cells were cultured to reach 100% confluence. Subsequently, the cell monolayer was scraped and the cells were maintained in serum-free medium for 0 and 48 h at 37˚C. At each time point, images were captured at the same location under a light microscope (Leica Microsystems GmbH).

Subcutaneous tumor model. All animal experiments were approved by the Institutional Animal Care and Use Committee of Chongqing Medical University (approval no. IACUC-CQMU-2025-0457; Chongqing, China). In the present study, 4-6-week-old female BALB/c mice (weight, 14-18 g) were obtained from and raised at the Experimental Animal Center of Chongqing Medical University at a room temperature of 20-24˚C and 45-55% humidity under a 12-h light/dark cycle, with free access to water and food. Using the random number method, a total of eight mice were randomly divided into two groups: Vector and CKAP2L groups (n=4 mice/group). Briefly, CT26 cells ($2x10^6$) were stably infected with CKAP2L-OE and vector lentiviruses as aforementioned and then suspended in 100 μl PBS. This mix was subcutaneously injected into the right flank of each mouse, after which, tumor growth was independently and blindly measured every 3 days by two experimenters. The mice were continuously fed for 21 days, and the tumor size, health and behavior of the mice were checked every 1-2 days. The maximum allowable tumor diameter was 15 mm. When the tumor size reached 15 mm, when ulceration occurred on the body surface, or when the mice exhibited weakness, poor appetite and symptoms such as convulsions, tremors and paralysis, the experiment was terminated and euthanasia was performed. In the current study, no mice reached the aforementioned humane endpoints. Euthanasia was performed by intraperitoneal injection of an overdose of sodium pentobarbital (150 mg/kg), followed by confirmation of respiratory cessation, cardiac arrest and loss of vital reflexes. Subsequently, the tumors were removed and weighed.

Statistical analysis. GraphPad Prism 10 (Dotmatics) and SPSS 27 (IBM Corp.) software were used for statistical analyses. Each experiment was independently repeated three times and all data are presented as the mean ± standard deviation. Unpaired Student's t-test was used to analyze the differences between two groups, whereas one-way ANOVA followed by Dunnett's test was used to analyze the differences among multiple groups. For comparisons among multiple groups with two treatment factors, two-way ANOVA followed by Tukey test was adopted. Adjusted $P<0.05$ was considered to indicate a statistically significant difference.

Results

Association between smoking and CRC. Among the participants with CRC, 60.5% of them had reported a history of smoking and 24.1% had reported secondhand smoke exposure (Table SI). A positive link between smoking and CRC was determined by logistic regression analyses (Table I). After fully adjusting for covariates, the risk of CRC in the past smoking [odds ratio (OR), 1.595; 95% confidence interval (CI), 1.020-2.493] and current smoking (OR, 1.738; 95% CI, 1.033-2.923) groups was higher than that reported in the no smoking history group. No difference in the risk of CRC was observed between the secondhand smoking and no smoking groups (OR, 1.184; 95% CI, 0.706-1.984).

Serum cotinine, a major metabolite of nicotine, was used to assess the short-term smoke exposure levels, and was classified as <0.015, 0.015-2.99, 3-10 and ≥10 ng/ml. In all models, no difference was observed among patients with different cotinine levels (Table I). The effect of age at the start of smoking cigarettes regularly on the risk of CRC was also explored; notably, no difference among patients in the different age groups was observed in all models (Table I).

Causality of smoking and CRC. A total of 52 IVs were included in MR analysis of cigarettes per day. MR analysis confirmed that cigarettes per day had a causal effect on CRC (IVW_FE: OR, 1.278; 95% CI, 1.030-1.586; IVW_MRE: OR, 1.278; 95% CI, 1.079-1.515) (Fig. 1). No heterogeneity (Cochran's Q test, P=0.982), pleiotropy (MR-Egger intercept, P=0.676) and outliers (MR-PRESSO, P=0.977) were observed, which confirmed the reliability of the results (Table SII).

A total of 8, 21, 331 and 13 IVs were included for the age of initiation of regular smoking, smoking cessation, smoking initiation and pack years of adult smoking, respectively. No causality was observed between these factors and CRC (all $P>0.05$; Fig. 1). No heterogeneity, pleiotropy and outliers were observed in these MR analyses. The details of Cochran's Q test, MR-Egger intercept and MR-PRESSO are listed in Table SII.

Table I. Association between smoking and colorectal cancer.

	Non-adjusted model		Adjusted model I		Adjusted model II	
Characteristic	OR (95% CI)	P-value	OR (95% CI)	P-value	OR (95% CI)	P-value
Smoking						
No smoking	Ref		Ref		Ref	
Past smoking	2.208 (1.489, 3.273)	0.0001	1.684 (1.111, 2.552)	0.0154	1.595 (1.020, 2.493)	0.0429
Current smoking	0.824 (0.506, 1.342)	0.4377	1.786 (1.106, 2.885)	0.0191	1.738 (1.033, 2.923)	0.0394
Secondhand smoking	0.860 (0.516, 1.431)	0.5619	1.179 (0.708, 1.962)	0.5285	1.184 (0.706, 1.984)	0.5237
Cotinine, ng/ml						
<0.015	Ref		Ref		Ref	
0.015-2.99	0.612 (0.169, 2.210)	0.4545	0.634 (0.175, 2.301)	0.4900	0.626 (0.173, 2.258)	0.4753
3-10	1.517 (1.043, 2.208)	0.0310	0.823 (0.557, 1.215)	0.3277	0.847 (0.575, 1.248)	0.4035
≥10	1.786 (1.168, 2.729)	0.0083	0.732 (0.475, 1.127)	0.1589	0.752 (0.478, 1.184)	0.2209
Age at which started smoking cigarettes regularly						
Never regularly smoked	Ref		Ref		Ref	
<20 years	0.999 (0.360, 2.776)	0.9986	1.042 (0.361, 3.005)	0.9400	1.059 (0.365, 3.074)	0.9169
≥20 years	1.335 (0.460, 3.872)	0.5963	0.986 (0.327, 2.972)	0.9794	1.006 (0.335, 3.025)	0.9916

Non-adjusted model was adjusted for no variables; adjusted model I was adjusted for age, sex and ethnicity; adjusted model II was adjusted for age, sex, ethnicity, education, marital status, ratio of family income to poverty, body mass index and alcohol consumption. CI, confidence interval; OR, odds ratio.

CSE promotes CRC progression. After 4 days of treatment with CSE, compared with that in the control group, treatment with CSE increased cell viability; among all groups, CSE concentrations of 0.125 and 0.25% had the highest capacity to promote cell viability in all three cell lines, as confirmed by CCK8 (Fig. 2A). In groups treated with 4% CSE, cell viability was not significantly promoted. Therefore, in the subsequent experiments, CSE concentrations of 0.125 and 0.25% were selected to establish the chronic smoke exposure model, and were used for functional experiments on RKO and HCT116 cells. Among the three cell lines, RKO and HCT116 cells showed a more significant increase in cell proliferation after short-term CSE treatment, and were selected for subsequent experiments.

Transwell assays revealed that smoke exposure increased the number of migratory and invasive RKO and HCT116 cells (Fig. 2B). The EdU assay also showed that smoke exposure significantly stimulated the proliferation of CRC cells (Fig. 2C). Moreover, smoke exposure promoted the protein expression levels of N-cadherin and Vimentin, but inhibited the expression levels of E-cadherin, indicating that CSE promoted epithelial-mesenchymal transition (EMT) (Fig. 2D). These results suggested that CSE promotes CRC cell progression and increases the expression of CKAP2L.

Identifying key genes related to both smoking and CRC. The scRNA-seq analysis identified 2,450 DEGs in the epithelial cells of CRC. Subsequently, 677 upregulated DEGs were screened from the bulk RNA-seq and 2,973 upregulated DEGs were filtered out from TCGA dataset. To further identify genes related to CRC, 245 genes were identified using the WGCNA method based on TCGA dataset. Based on TCGA, scRNA-seq and bulk RNA-seq datasets, a total of 12 CRC-related genes were screened out by overlapping the aforementioned DEGs (Fig. 3A).

By performing RNA-seq in CSE-treated HCT116 cells, 1,663 upregulated genes were identified in the CSE-treated group as smoking-related genes. Finally, six key genes involved in smoking-enhanced CRC progression were selected by overlapping CRC-related genes and smoking-related genes, including CENPW, FOXM1, MAD2L1, CKAP2L, CEP55 and ECT2 (Fig. 3A).

Among these six key genes, CKAP2L is an emerging cell cycle-related gene (19). Moreover, both the mRNA and protein expression levels of CKAP2L were upregulated by CSE treatment (P<0.05; Figs. 2D and 3B). These results suggested that CKAP2L may be a critical molecule in smoking-enhanced CRC progression.

Verification of CKAP2L expression. As shown in Fig. 3B and C, both the mRNA and protein expression levels of CKAP2L were higher in CRC cells than in normal colonic cells. Furthermore, CKAP2L expression was higher in Caco-2 and RKO cells, but lower in HCT116 cells. Therefore, knockdown of CKAP2L was performed in Caco-2 and RKO cells, and overexpression of CKAP2L was performed in HCT116 cells. The most effective shRNA plasmids (shCKAP2L #1 and #2) were determined by RT-qPCR and western blotting, and were used in subsequent experiments. The expression of CKAP2L was significantly suppressed and upregulated

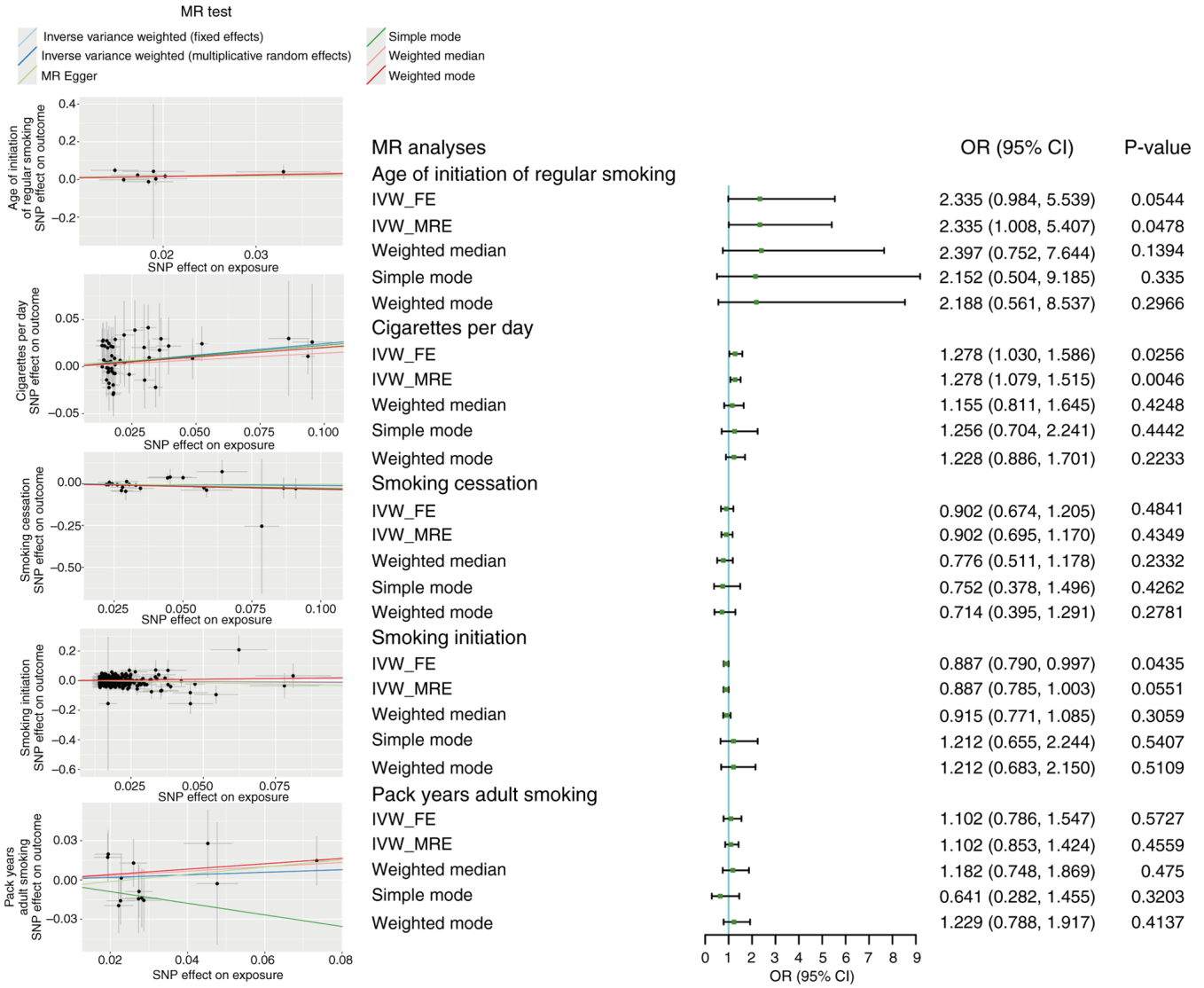

Figure 1. Scatter plots and forest plot showing the results of MR analyses. CI, confidence interval; FE, fixed effect; IVW, inverse variance weighted; MR, Mendelian randomization; MRE, multiplicative random effect; OR, odds ratio; SNP, single-nucleotide polymorphism.

following transduction with shCKAP2L #1 and #2, and the CKAP2L-OE plasmid, respectively (Fig. 3B and C).

CKAP2L promotes cell migration and invasion. Wound healing assay confirmed that knockdown of CKAP2L inhibited the migratory ability of RKO cells (P<0.05; Fig. 4A). By contrast, promotion of migration was observed in HCT116 cells after CKAP2L overexpression (P<0.05; Fig. 4A). The same trend in migration and invasion was confirmed by Transwell assay (Fig. 4B). Western blotting revealed that knockdown of CKAP2L enhanced E-cadherin expression, and suppressed N-cadherin and Vimentin expression (Fig. 4C), whereas overexpression of CKAP2L showed the opposite trend. These results revealed that CKAP2L may enhance the migration and invasion of CRC cells by promoting EMT.

CKAP2L promotes cell proliferation. The proliferation of cells *in vitro* was confirmed by EdU, CCK8 and colony formation assays. Notably, EdU (Fig. 5A), CCK8 (Fig. 5B) and colony formation (Fig. 5C) assays showed that knockdown of CKAP2L significantly suppressed the proliferation of Caco-2 and RKO cells. By contrast, overexpression of CKAP2L promoted the proliferation of HCT116 cells.

Flow cytometry confirmed that knockdown of CKAP2L significantly reduced the proportion of cells in G_2 and S phases, whereas the opposite trend was shown after CKAP2L overexpression (Fig. 5D).

Cell proliferation *in vivo* was confirmed by animal experiments. After stable transduction of CT26 cells with the CKAP2L-OE plasmid (Fig. S1A), these cells were used to establish a subcutaneous tumor model. Among all groups, the measured diameter of the largest tumor was 12 mm, and the maximum volume was 486 mm^3. The results showed that overexpression of CKAP2L increased formed tumor weight (mean, 225.0 vs. 457.5 mg; 95% CI, 14.81-450.2; P=0.0399; Fig. 5E). These results supported that CKAP2L can promote the proliferation of CRC cells *in vivo*.

Further western blotting results revealed that knockdown of CKAP2L inhibited the expression of cyclin A2, cyclin B1, CDK1 and CDK2, and promoted the expression of cyclin D1,

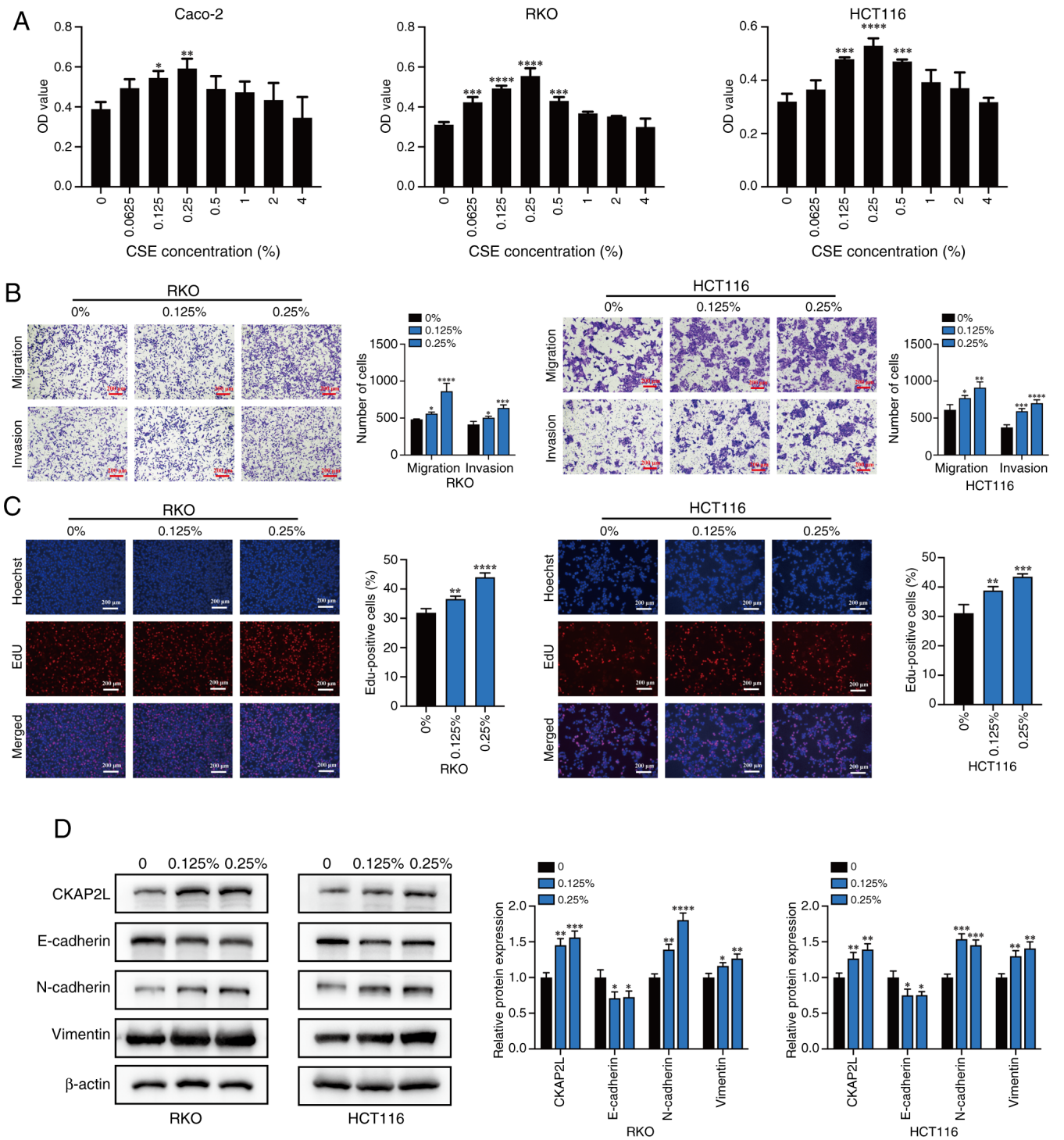

Figure 2. Treatment with CSE promotes the proliferation and metastasis of CRC cells. (A) Viability of CRC cells (Caco-2, RKO and HCT116) treated with CSE for 4 days was measured by Cell Counting Kit 8. (B) Migration and invasion of CRC cells (RKO and HCT116) treated with CSE for 2 months were measured using Transwell assay (x100 magnification). (C) Proliferation of CRC cells (RKO and HCT116) treated with CSE for 2 months was measured with EdU (x200 magnification). (D) Relative protein expression levels in CRC cells treated with CSE for 2 months. Data were analyzed using one-way ANOVA followed by Dunnett's test. *P<0.05, **P<0.01, ***P<0.001 and ****P<0.0001 vs. control (0% CSE). CKAP2L, cytoskeleton-associated protein 2-like; CRC, colorectal cancer; CSE, cigarette smoke extract; EdU, 5-ethynyl-2'-deoxyuridine.

whereas overexpression of CKAP2L generated the opposite results (Fig. 5F). These results suggested that CKAP2L promotes CRC cell proliferation by regulating the cell cycle.

CKAP2L promotes CRC progression by upregulating AREG expression. To explore the molecular mechanism by which CKAP2L promotes the progression of CRC, RNA-seq was performed on CRC cells that had been transfected with shCKAP2L and CKAP2L-OE plasmids (Fig. 6A). Subsequently, 20 key genes were filtered out by overlapping upregulated DEGs in CKAP2L-OE cells, downregulated DEGs in shCKAP2L cells and upregulated DEGs in HCT116-CSE

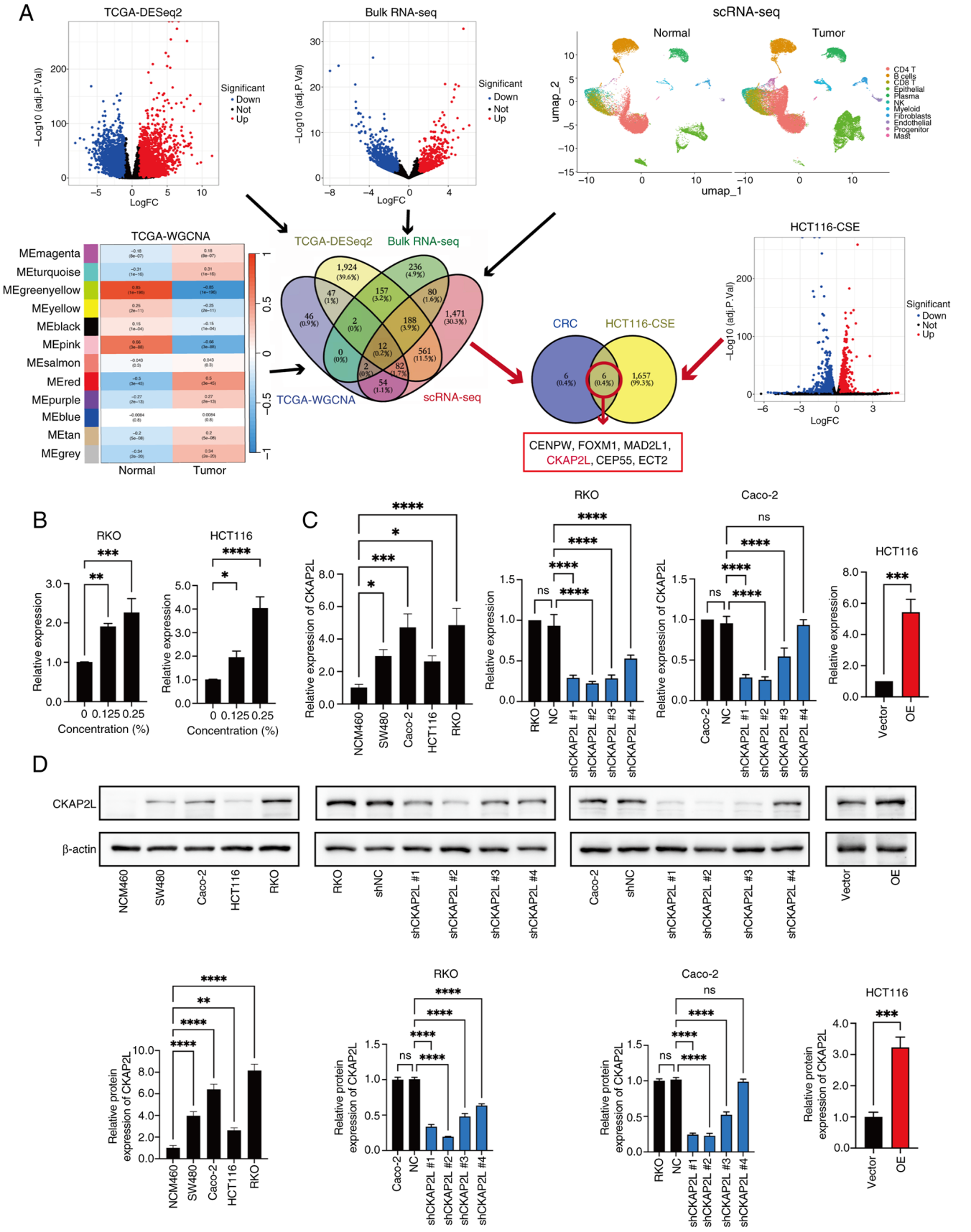

Figure 3. Bioinformatics analyses and investigation of CKAP2L expression. (A) Identification of key genes involved in smoking-enhanced CRC progression. (B) Relative expression of CKAP2L in CRC cells treated with CSE for 2 months detected by reverse transcription-quantitative PCR and normalized against β-actin. (C) Expression of CKAP2L was measured by reverse transcription-quantitative PCR in colorectal cell lines and transduced CRC cells. (D) CKAP2L expression was measured by western blotting in colorectal cell lines and transduced CRC cells. Data were analyzed using one-way ANOVA followed by Dunnett's test for multiple groups, or unpaired Student's t-test for two groups. *P<0.05, **P<0.01, ***P<0.001 and ****P<0.0001. CKAP2L, cytoskeleton-associated protein 2-like; CRC, colorectal cancer; CSE, cigarette smoke extract; FC, fold change; NC, negative control; OE, over expression; RNA-seq, RNA sequencing; scRNA-seq, single-cell RNA-seq; sh, short hairpin; TCGA, The Cancer Genome Atlas.

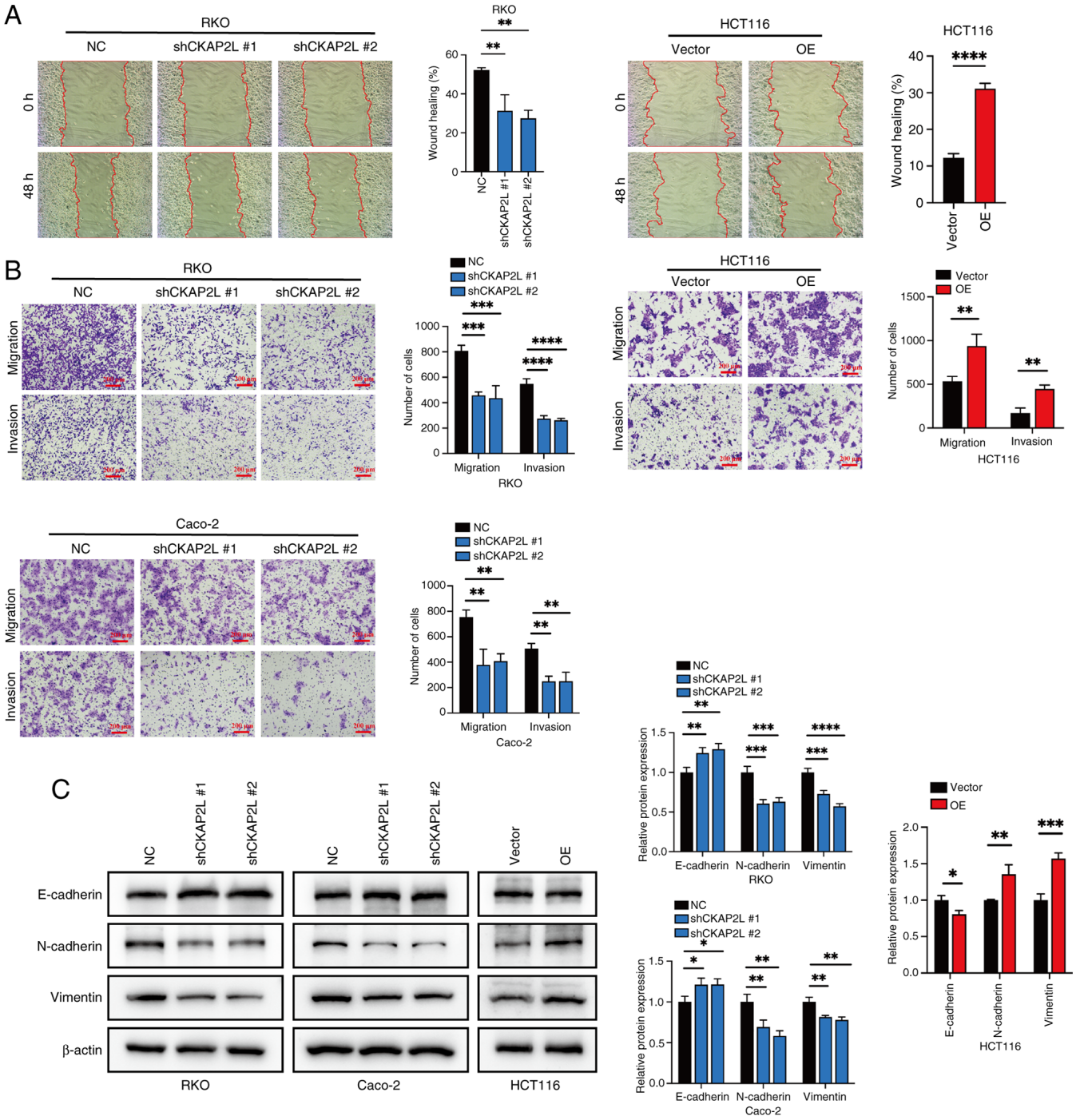

Figure 4. CKAP2L promotes cell migration and invasion in colorectal cancer cells. (A) Wound healing results for transduced cells (x100 magnification). (B) Transwell assay results for transduced cells (x100 magnification). (C) Western blot analysis results for transduced cells. Data were analyzed using one-way ANOVA followed by Dunnett's test for multiple groups, or unpaired Student's t-test for two groups. *P<0.05, **P<0.01, ***P<0.001 and ****P<0.0001. CKAP2L, cytoskeleton-associated protein 2-like; NC, negative control; OE, overexpression; sh, short hairpin.

cells (Fig. 6B). Among these 20 key genes regulated by CKAP2L, AREG is a biomarker for cancer progression (45), indicating that CKAP2L can regulate the expression of AREG to promote CRC progression. The effect of CSE on AREG expression was then assessed; the mRNA levels of AREG were upregulated by CSE treatment (Fig. 6C) and CKAP2L overexpression (Fig. 6D). However, after successfully inhibiting AREG expression via transfection of cells with siAREG (Fig. S1B), the expression of CKAP2L did not change (Fig. 6D). ELISA confirmed that overexpression of CKAP2L also promoted the secretory protein levels of AREG (Fig. 6E). These results reveled that smoking may upregulate AREG expression by increasing the expression levels of CKAP2L.

To evaluate whether CKAP2L promotes CRC progression by upregulating the expression of AREG, CCK8 and Transwell assays were conducted. As shown in Fig. 6F, AREG knockdown partially suppressed the enhanced proliferative ratio of CRC cells caused by overexpression of CKAP2L. Transwell assay results confirmed that knockdown of AREG expression decreased the number of migratory

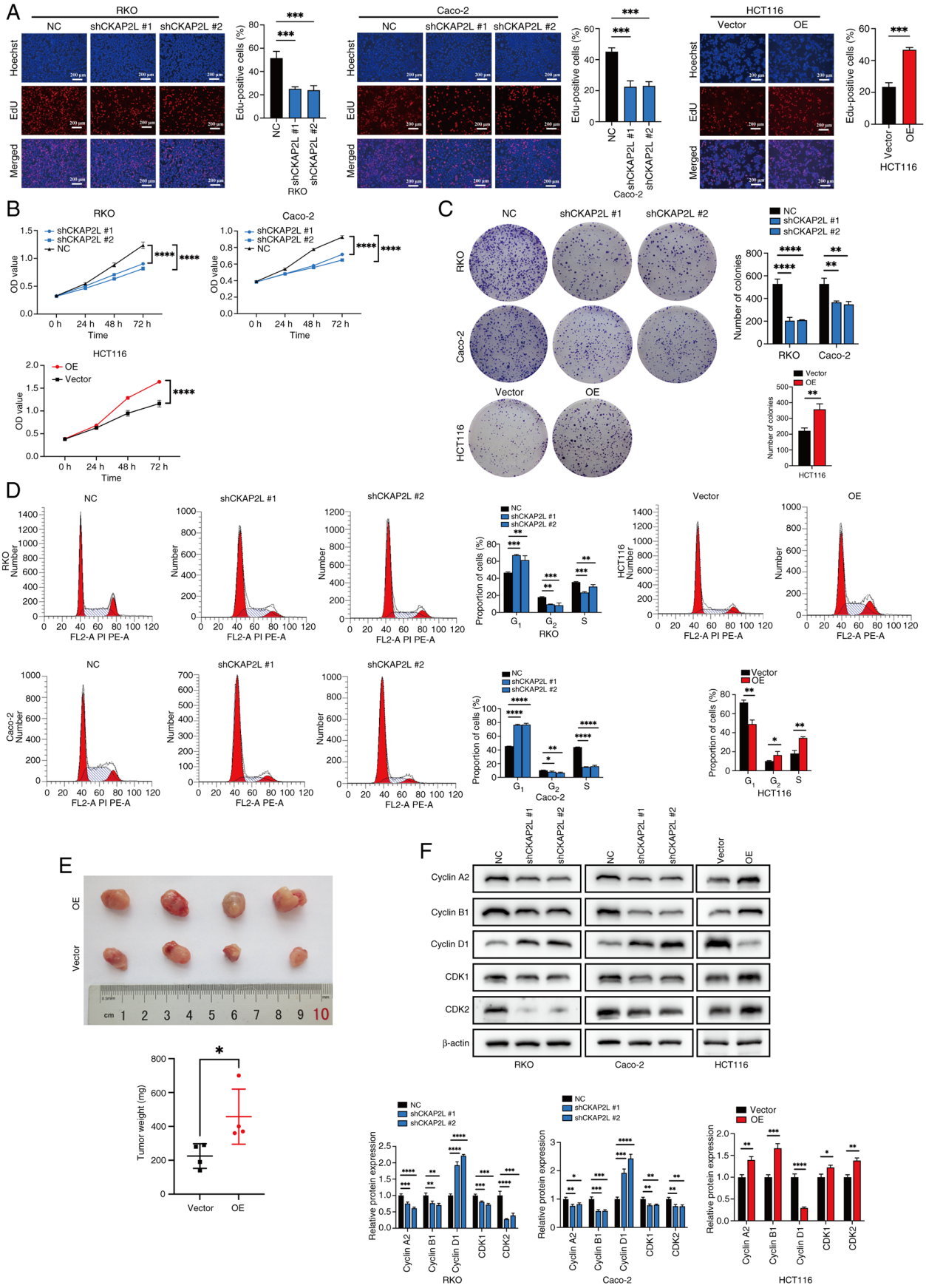

Figure 5. CKAP2L promotes the proliferation of colorectal cancer cells. (A) Proliferation of transduced cells was measured using the (A) EdU (x200 magnification), (B) Cell Counting Kit-8 or (C) colony formation assays. (D) Results of cell cycle analysis of transduced cells. (E) Cell proliferation *in vivo* was measured using a subcutaneous tumor model. (F) Expression of cell cycle-related proteins was measured by western blotting. Data were analyzed using (A and C-F) one-way ANOVA followed by Dunnett's test for multiple groups, or unpaired Student's t-test for two groups; or (B) two-way ANOVA followed by Tukey test. *P<0.05, **P<0.01, ***P<0.001 and ****P<0.0001. CKAP2L, cytoskeleton-associated protein 2-like; EdU, 5-ethynyl-2'-deoxyuridine; NC, negative control; OE, overexpression; sh, short hairpin.

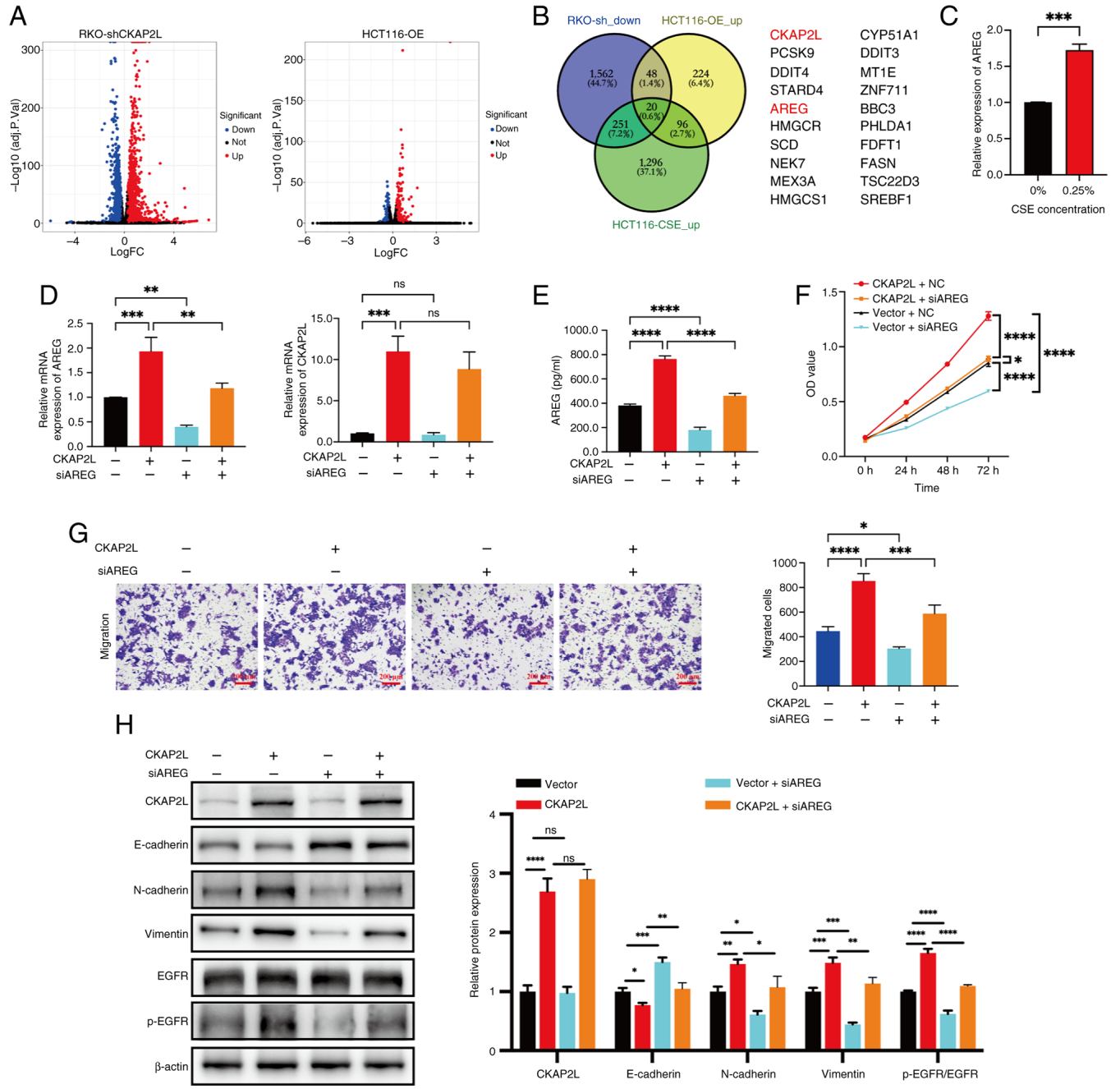

Figure 6. CKAP2L promotes proliferation and migration of CRC cells by promoting AREG expression. (A) RNA sequencing results for transduced CRC cells. (B) Venn diagram shows the overlapping genes between transduced cells and CSE-treated HCT116 cells. (C) Relative expression of AREG in CRC cells treated with CSE detected by RT-qPCR and normalized against β-actin. (D) Relative expression levels of AREG and CKAP2L were detected by RT-qPCR and normalized against β-actin. (E) Secreted protein levels of AREG were detected by enzyme-linked immunosorbent assay. (F) Proliferation of transduced/transfected cells was measured by Cell Counting Kit 8. (G) Migration of transduced/transfected cells was measured by Transwell assay (x100 magnification). (H) Expression levels of proteins were measured by western blotting. Data were analyzed using two-way ANOVA followed by Tukey test, or unpaired Student's t-test for two groups. *P<0.05, **P<0.01, ***P<0.001 and ****P<0.0001. AREG, amphiregulin; CKAP2L, cytoskeleton-associated protein 2-like; CRC, colorectal cancer; CSE, cigarette smoke extract; EGFR, epidermal growth factor receptor; NC, negative control; OE, overexpression; p-, phosphorylated; RT-qPCR, reverse transcription-quantitative PCR; sh, short hairpin; si, small interfering.

cells induced by CKAP2L overexpression (Fig. 6G). Western blotting further confirmed that inhibiting the expression of AREG partially restored the upregulated protein levels of N-cadherin and Vimentin and phosphorylation level of EGFR, and downregulated the protein levels of E-cadherin caused by overexpression of CKAP2L (Fig. 6H). These results suggested that CKAP2L may promote CRC progression by activating the AREG/EGFR pathway.

CKAP2L increases STAT3 phosphorylation to promote the expression of AREG. After overexpression of CKAP2L, the phosphorylation level of STAT3 increased, whereas the opposite occurred when CKAP2L was knocked down, as determined by western blotting (Fig. 7A). To explore whether CKAP2L promotes CRC progression by enhancing STAT3 phosphorylation, the STAT3 phosphorylation inhibitor Stattic was used. After culturing HCT116 cells in medium containing

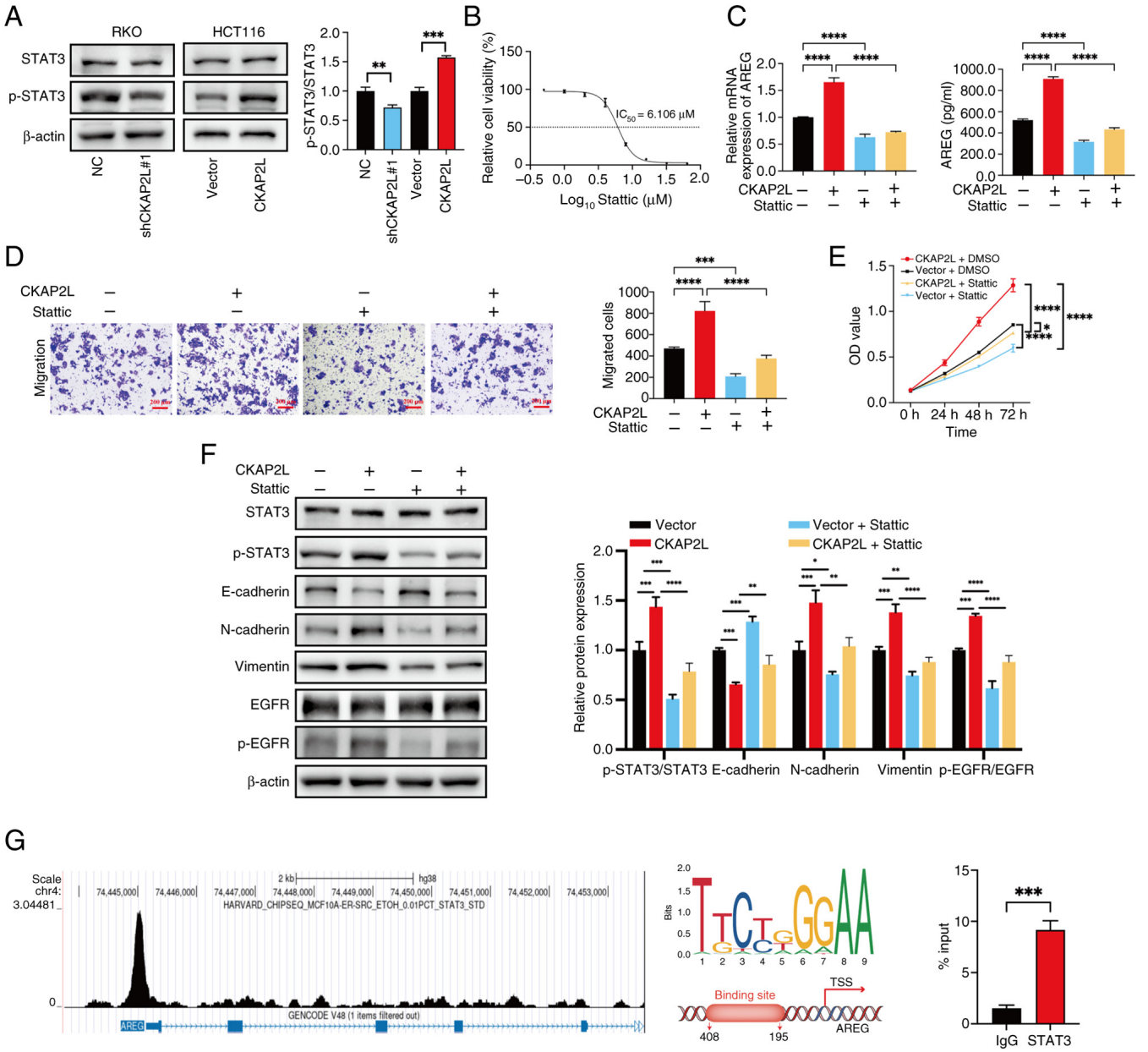

Figure 7. CKAP2L promotes proliferation and migration of colorectal cancer cells through the STAT3/AREG/EGFR axis. (A) Expression levels of STAT3 and p-STAT3 proteins measured by western blotting. (B) Calculation of IC_{50} in HCT116 cells treated with Stattic for 24 h. (C) Levels of AREG were measured by reverse transcription-quantitative PCR and enzyme-linked immunosorbent assay. (D) Migration of cells was detected by Transwell assay (x100 magnification). (E) Proliferation of cells was measured by Cell Counting Kit 8. (F) Expression levels of proteins measured by western blotting. (G) Binding peak of STAT3 on the promoter region of AREG was detected by Cistrome Data Browser, the binding motif was predicted using the JASPAR database, and the binding of STAT3 to the AREG promoter was evaluated by chromatin immunoprecipitation assay. Data were analyzed using (A and G) Unpaired Student's t-test, and (C-F) two-way ANOVA followed by Tukey test. *P<0.05, **P<0.01, ***P<0.001 and ****P<0.0001. AREG, amphiregulin; CKAP2L, cytoskeleton-associated protein 2-like; EGFR, epidermal growth factor receptor; NC, negative control; p-, phosphorylated; sh, short hairpin; STAT3, signal transducer and activator of transcription 3; TSS, transcription start site.

Stattic for 24 h, cell proliferation was measured using CCK8 to calculate the IC_{50}; the results showed that the IC_{50} of Stattic was 6.106 μM (Fig. 7B). Both RT-qPCR and ELISA confirmed that Stattic inhibited AREG levels enhanced by CKAP2L overexpression (Fig. 7C). Furthermore, Transwell and CCK8 assays indicated that treatment with Stattic inhibited the migration and proliferation of HCT116 cells enhanced by overexpression of CKAP2L (Fig. 7D and E). Western blotting revealed that suppression of STAT3 phosphorylation inhibited the protein expression levels of N-cadherin and Vimentin and the phosphorylation level of EGFR enhanced by CKAP2L overexpression, and restored the expression level of E-cadherin downregulated by CKAP2L overexpression (Fig. 7F). These results indicated that CKAP2L may promote AREG expression by increasing the phosphorylation of STAT3.

The current study further investigated the interaction between STAT3 and AREG. The Cistrome Data Browser showed that STAT3 has a significant binding peak in the promoter region of AREG, suggesting that STAT3 is a transcription factor of AREG (Fig. 7G). Subsequently, the binding motif of STAT3 and the potential binding site was predicted by JASPAR database. ChIP-qPCR assay confirmed

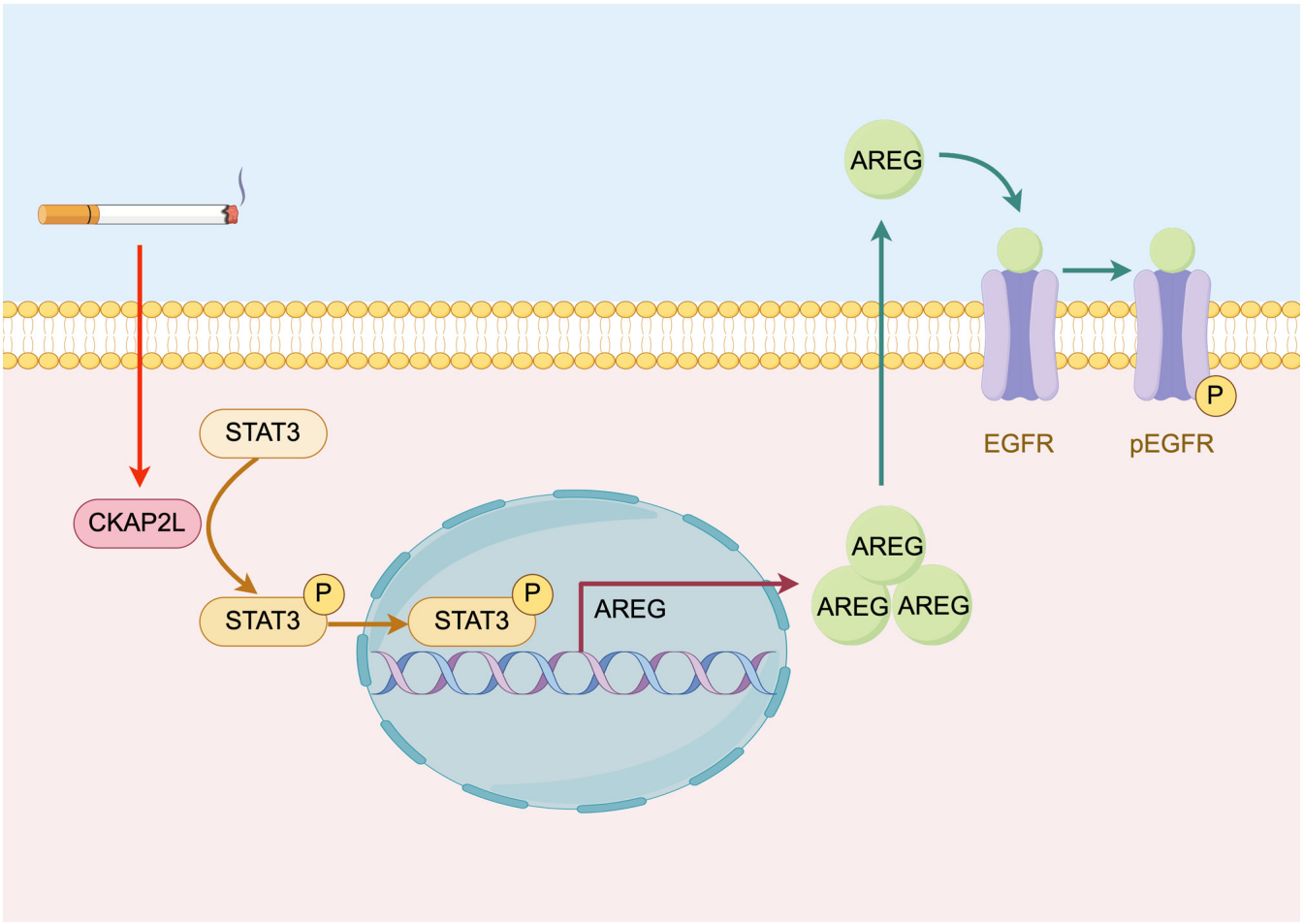

Figure 8. Smoking may promote colorectal cancer progression through the CKAP2L/STAT3/AREG/EGFR axis. This figure was drawn by Figdraw (https://www.figdraw.com/). AREG, amphiregulin; CKAP2L, cytoskeleton-associated protein 2-like; EGFR, epidermal growth factor receptor; STAT3, signal transducer and activator of transcription 3.

the significant enrichment of STAT3 on the promoter region of AREG (Fig. 7G). These results confirmed that STAT3 is a transcription factor of AREG.

These results revealed that CKAP2L may promote the phosphorylation level of STAT3. Subsequently, STAT3 promotes AREG transcription and activates the AREG/EGFR pathway, resulting in CRC progression (Fig. 8).

Discussion

Smoking is a major risk factor for CRC that also affects the survival of patients with CRC (46-49). In a previous study, a cigarette smoke-exposed C57BL/6 mice model demonstrated that cigarette smoke promotes CRC progression by modulating the gut microbiota and related metabolites (9). Tumor immunity serves a crucial role in the progression of cancer and some inflammatory markers, such as albumin-to-globulin ratio and neutrophil percentage to albumin ratio, are notably associated with the prognosis of CRC (50). It has been shown that smoking is markedly associated with reduced macrophage densities and T-lymphocyte response in patients with CRC, which contributes to CRC carcinogenesis (51,52). Smoking is also positively associated with high CpG island methylation, BRAF mutations and high microsatellite instability, which increases the risk of CRC (53). In the present study, the cross-sectional study confirmed that past smoking and current smoking were significantly linked with a higher CRC risk compared with not smoking. In addition, the ORs of the current smoking group were higher than those of the past smoking group, indicating a reduced risk of CRC after smoking cessation. However, no difference in CRC risk was observed between secondhand smoking and no smoking. A previous study also reported that harmful associations between secondhand smoking and cancer were supported by weak evidence (54). Moreover, no significant relationship between CRC and cotinine levels was observed, suggesting that short-term smoking exposure levels had no effect on CRC risk. Analysis of the age at which individuals started smoking cigarettes regularly also showed no significant relationship with CRC risk. Previous MR analyses have reported the causality between smoking and CRC (7,55). In the current study, the causality between cigarettes per day and CRC was also confirmed by MR analysis. Consistent with previous studies, these results confirmed that smoking is positively linked to CRC risk, and a causality exists between the two, whereas quitting smoking can reduce this risk. These results revealed the positive association between smoking and CRC.

To investigate the hypothesis in various subtypes of CRC, four CRC cell lines were selected for use in the subsequent experiments. SW480 cells were selected as a model of primary colorectal adenocarcinoma; this cell line harbors a KRAS G12D mutation and a p53 R273H mutation, representing common oncogenic drivers in CRC. HCT116 cells were selected as a model of mismatch repair-deficient/microsatellite instability-high (MSI-H) CRC; this cell line carries an activating KRAS G12D mutation. RKO cells were selected as another model of MSI-H CRC, which carries a wild-type APC gene that is distinct from numerous other CRC cell lines. Caco-2 cells were selected due to their unique ability to spontaneously differentiate into enterocyte-like cells. By using these cell lines, the current study aimed to ensure that the findings were robust and not limited to a single genetic subtype of CRC.

The CSE treatment cell model was constructed to assess the direct effect of cigarette smoke on CRC cells. In the present study, CSE concentrations of 0.125 and 0.25% were selected by CCK8 (cells treated with 0.125 and 0.25% CSE showed peak proliferation) to establish the chronic CSE treatment model according to previous studies (18,37,56). Assuming that the blood volume of an adult is 5,000 ml, one cigarette dissolved in the blood is equal to 0.20% CSE. Therefore, CSE concentrations of 0.125 and 0.25% are approximately equal to the physiological exposure concentration and were selected to establish the chronic CSE treatment model. The EdU assay was also employed to detect the cytotoxicity of CSE, rather than only the short-term CCK8 assay. The results confirmed an increase in viable cell number in the CSE treatment groups without causing notable cell death. In the chronic CSE treatment model, smoke exposure enhanced CRC cell proliferation, migration and invasion, and increased the expression of proliferation-related proteins (cyclin A2, cyclin B1, CDK1 and CDK2) and EMT-associated proteins (N-cadherin and Vimentin). These results suggested that smoking may enhance CRC cell progression.

RNA-seq was conducted on CSE-treated HCT116 cells and it was revealed that CKAP2L may be a critical gene involved in smoking-enhanced CRC. Radmis, the mouse ortholog of CKAP2L, has been identified as a novel microtubule-associated protein by Yumoto *et al* (57). Notably, scaffold proteins are involved in promoting tumor progression and metabolic adaptation (58). Previous bioinformatics analyses have identified CKAP2L as a hub gene in multiple types of cancer (such as CRC and clear cell renal cell carcinoma) (59,60), and the expression of CKAP2L has been shown to be upregulated in tumor tissues, leading to a poor prognosis (61,62). Mechanistically, CKAP2L serves a vital role in regulating the cell cycle and the tumor immune microenvironment, thereby promoting the progression of cancer cells (63,64). The present study reported that CKAP2L expression in CRC cells was significantly upregulated by CSE treatment. Furthermore, overexpression of CKAP2L enhanced the proliferation, migration and invasion of CRC cells. Cell cycle analysis also revealed that CKAP2L was involved in regulation of S and G_2/M phases. Moreover, CKAP2L increased the levels of EMT-, and S and G_2/M phase-related proteins (for example, N-cadherin, Vimentin, cyclin A2, cyclin B1, CDK1 and CDK2). These results confirmed that CKAP2L is upregulated by smoking, promoting CRC progression through its regulation of the cell cycle.

By regulating CKAP2L expression, both the mRNA and protein expression levels of AREG were affected. AREG is an EGFR ligand, that mainly serves its role by interacting with EGFR (65). EGFR has an important role in CRC progression and is a fundamental therapeutic target (66). The AREG/EGFR axis is involved in regulating proliferation, metastasis, tumor microenvironment and tumor immune tolerance in multiple tumors, such as melanoma and esophageal squamous cell carcinoma (45,67,68). The present study revealed that CKAP2L could upregulate AREG expression, leading to the promotion of EGFR phosphorylation and activation of the AREG/EGFR signaling pathway. Further experiments are needed to explore the downstream EGFR pathways that are involved in smoking-enhanced CRC progression. Furthermore, the knockdown of AREG only partially inhibited the cell proliferation and migration induced by CKAP2L, indicating that there are other downstream pathways involved. Other mechanisms still require further investigation.

To explain how CKAP2L promote the expression of AREG, a ChIP assay was performed. The results revealed that CKAP2L increased STAT3 phosphorylation, leading to the progression of CRC cells. STAT3 is a classic transcription factor that participates in the regulation of almost all malignant characteristics of tumors (69-71) and is also a therapeutic target for patients with CRC (72). Inhibiting the phosphorylation of STAT3 was shown to suppress the expression of AREG, which verified the regulatory effect of STAT3 on AREG. Moreover, the results of the ChIP assay confirmed that STAT3 promoted AREG transcription by binding to its promoter region.

The present study confirmed the positive association between smoking and CRC. In addition, the study explored the influence of smoking features on CRC. Further experiments also revealed that smoke exposure may stimulate CRC progression through the CKAP2L/STAT3/AREG/EGFR axis.

Notably, there are several limitations in the present study. Self-reported NHANES data may introduce recall bias. Moreover, there was a lack of detailed clinicopathological information about cancer, such as stage, therapies, drug resistance and prognosis, which limits comprehensive evaluation of the impact of smoking on CRC. Furthermore, some confounders not included in this cross-sectional analysis may affect the link between smoking and CRC. Due to the lack of information about electronic cigarettes during the period of 1999-2014, the present study did not collect or analyze data related to electronic cigarettes. For MR analysis, GWAS data from Europe limits the generalizability of these MR analysis results to other populations, and the brands and formulations of cigarettes may lead to differences in the experimental results. Moreover, CSE cannot fully replicate human smoking exposure conditions. Further experiments are needed to explore the downstream EGFR pathways and other mechanisms involved in smoking-enhanced CRC.

In conclusion, the current study demonstrated that both past smoking and current smoking are positively related to CRC, and identified a causality between smoking and CRC. CSE promoted the expression of CKAP2L, which regulated the cell cycle, and promoted the proliferation, migration and invasion of

CRC cells. These findings revealed that smoke exposure may enhance CRC progression through CKAP2L/AREG signaling.

Acknowledgements

Not applicable.

Funding

The present study was supported by the China Early Gastrointestinal Cancer Physician Common Growth Program (grant no. GTCZ-2024-08).

Availability of data and materials

The RNA-seq data generated in the present study may be found in the Gene Expression Omnibus database under accession numbers GSE305020 and GSE305039, or at the following URLs: https://www.ncbi.nlm.nih.gov/geo/query/acc.cgi?acc=GSE305020, https://www.ncbi.nlm.nih.gov/geo/query/acc.cgi?acc=GSE305039. Other data generated in the present study are available from the corresponding author.

Authors' contributions

SW contributed to study design, carried out the cross-section and Mendelian randomization analyses, performed cell experiments and wrote the main manuscript. FW performed the bioinformatics analysis and animal experiment, and was a major contributor in writing the manuscript. XL, ZhiJ and FL performed cell experiments, data collection and analysis. ZheJ designed the study and was involved in revising the manuscript. SW and ZheJ confirm the authenticity of all the raw data. All authors read and approved the final manuscript.

Ethics approval and consent to participate

Animal experiments were approved by the Institutional Animal Care and Use Committee of Chongqing Medical University (approval no. IACUC-CQMU-2025-0457).

Patient consent for publication

Not applicable.

Competing interests

The authors declare that they have no competing interests.

References

1. Harris E: Cancer risk decreased 10 years after quitting smoking. JAMA 331: 822, 2024.
2. Park E, Kang HY, Lim MK, Kim B and Oh JK: Cancer risk following smoking cessation in Korea. JAMA Netw Open 7: e2354958, 2024.
3. Hecht SS and Hatsukami DK: Smokeless tobacco and cigarette smoking: Chemical mechanisms and cancer prevention. Nat Rev Cancer 22: 143-155, 2022.
4. Jiang M, Han J, Ma Q, Chen X, Xu R, Wang Q, Zheng J, Wang W, Song J, Huang Y and Chen Y: Nicotine-derived NNK promotes CRC progression through activating TMUB1/AKT pathway in METTL14/YTHDF2-mediated m6A manner. J Hazard Mater 467: 133692, 2024.
5. Siegel RL, Kratzer TB, Giaquinto AN, Sung H and Jemal A: Cancer statistics, 2025. CA Cancer J Clin 75: 10-45, 2025.
6. GBD 2019 Colorectal Cancer Collaborators: Global, regional, and national burden of colorectal cancer and its risk factors, 1990-2019: A systematic analysis for the global burden of disease study 2019. Lancet Gastroenterol Hepatol 7: 627-647, 2022.
7. Zhou X, Xiao Q, Jiang F, Sun J, Wang L, Yu L, Zhou Y, Zhao J, Zhang H, Yuan S, *et al*: Dissecting the pathogenic effects of smoking and its hallmarks in blood DNA methylation on colorectal cancer risk. Br J Cancer 129: 1306-1313, 2023.
8. Li H, Chen X, Hoffmeister M and Brenner H: Associations of smoking with early- and late-onset colorectal cancer. JNCI Cancer Spectr 7: pkad004, 2023.
9. Bai X, Wei H, Liu W, Coker OO, Gou H, Liu C, Zhao L, Li C, Zhou Y, Wang G, *et al*: Cigarette smoke promotes colorectal cancer through modulation of gut microbiota and related metabolites. Gut 71: 2439-2450, 2022.
10. Wu S and Wu F: Association of urinary incontinence with depression among men: A cross-sectional study. BMC Public Health 23: 944, 2023.
11. Wu S, Yuan G, Wu L, Zou L and Wu F: Identifying the association between depression and constipation: An observational study and Mendelian randomization analysis. J Affect Disord 359: 394-402, 2024.
12. Hsiao CC, Yang AM, Wang C and Lin CY: Association between glyphosate exposure and cognitive function, depression, and neurological diseases in a representative sample of US adults: NHANES 2013-2014 analysis. Environ Res 237: 116860, 2023.
13. Xie Z, Wang L, Sun M, Wang R, Li J, Wang X, Guo R, Dong Y, Wang Y and Li B: Mediation of 10-year cardiovascular disease risk between inflammatory diet and handgrip strength: Base on NHANES 2011-2014. Nutrients 15: 918, 2023.
14. Zhang H, Wu Z, Chen Q, Yu G, Chen L, Ma Y and Chen Y: Subtype-specific causal effects of hypothyroidism on obstructive sleep apnea: A bidirectional Mendelian randomization study. Medicine (Baltimore) 104: e43266, 2025.
15. Wu S, Wu F and Jiang Z: Identification of hub genes, key miRNAs and potential molecular mechanisms of colorectal cancer. Oncol Rep 38: 2043-2050, 2017.
16. Hussain MS, Battaglia A, Szczepanski S, Kaygusuz E, Toliat MR, Sakakibara S, Altmüller J, Thiele H, Nürnberg G, Moosa S, *et al*: Mutations in CKAP2L, the human homolog of the mouse Radmis gene, cause Filippi syndrome. Am J Hum Genet 95: 622-632, 2014.
17. Jakobsen L, Vanselow K, Skogs M, Toyoda Y, Lundberg E, Poser I, Falkenby LG, Bennetzen M, Westendorf J, Nigg EA, *et al*: Novel asymmetrically localizing components of human centrosomes identified by complementary proteomics methods. EMBO J 30: 1520-1535, 2011.
18. Wu F, Wu S, Huang Y, Xiao X, Yu H, Bai X, Zhang C, Feng Z, Li L, Mei Y, *et al*: Smoking promotes the progression of bladder cancer through FOXM1/CKAP2L axis. J Transl Med 23: 785, 2025.
19. Chen W, Wang Y, Wang L, Zhao H and Li X: CKAP2L promotes esophageal squamous cell carcinoma progression and drug-resistance by modulating cell cycle. J Oncol 2022: 2378253, 2022.
20. Monteverde T, Sahoo S, La Montagna M, Magee P, Shi L, Lee D, Sellers R, Baker AR, Leong HS, Fassan M and Garofalo M: CKAP2L promotes non-small cell lung cancer progression through regulation of transcription elongation. Cancer Res 81: 1719-1731, 2021.
21. Luo Q, Zhu B, Wang C and Wang Y: CKAP2L plays a pivotal role in colorectal cancer progression via the dual regulation of cell cycle and epithelial-mesenchymal transition. Discov Med 37: 182-192, 2025.
22. Kim TR, Son B, Lee CG and Park HO: Amphiregulin in fibrotic diseases and cancer. Int J Mol Sci 26: 6945, 2025.
23. Zhang Z, Li Z, Zhang X, Ye W, Chen J, Wang L, Lin Z, Li J and Li Z: Association between secondhand smoke and cancers in adults in the US population. J Cancer Res Clin Oncol 149: 3447-3455, 2023.
24. Dove MS, Dockery DW and Connolly GN: Smoke-free air laws and secondhand smoke exposure among nonsmoking youth. Pediatrics 126: 80-87, 2010.
25. Benowitz NL, Bernert JT, Caraballo RS, Holiday DB and Wang J: Optimal serum cotinine levels for distinguishing cigarette smokers and nonsmokers within different racial/ethnic groups in the United States between 1999 and 2004. Am J Epidemiol 169: 236-248, 2009.

26. Hou W, Chen S, Zhu C, Gu Y, Zhu L and Zhou Z: Associations between smoke exposure and osteoporosis or osteopenia in a US NHANES population of elderly individuals. Front Endocrinol (Lausanne) 14: 1074574, 2023.
27. Du X, Peng T, Ma L and Cheng G: Serum cotinine levels and adolescents' sleep health outcomes from NHANES 2005 to 2018. Sci Rep 14: 21076, 2024.
28. Hukkanen J, Jacob P III and Benowitz NL: Metabolism and disposition kinetics of nicotine. Pharmacol Rev 57: 79-115, 2005.
29. Chen FF, Klemperer EM, Erath TG, DeSarno M, Leventhal AM and Higgins ST: Age, cumulative psychosocial risk factors, and health disparities in U.S. adult cigarette smoking: 2002-2019. BMC Med 23: 664, 2025.
30. Reitsma MB, Flor LS, Mullany EC, Gupta V, Hay SI and Gakidou E: Spatial, temporal, and demographic patterns in prevalence of smoking tobacco use and initiation among young people in 204 countries and territories, 1990-2019. Lancet Public Health 6: e472-e481, 2021.
31. Taylor E, Tattan-Birch H, Oldham M, East K, Walsh H and Jackson S: Smoking and drinking among the Gypsy and Traveller communities: A population study in England. Addiction: February 17, 2026 (Epub ahead of print).
32. Liu M, Jiang Y, Wedow R, Li Y, Brazel DM, Chen F, Datta G, Davila-Velderrain J, McGuire D, Tian C, *et al*: Association studies of up to 1.2 million individuals yield new insights into the genetic etiology of tobacco and alcohol use. Nat Genet 51: 237-244, 2019.
33. Potenza A, Balestrieri C, Spiga M, Albarello L, Pedica F, Manfredi F, Cianciotti BC, De Lalla C, Botrugno OA, Faccani C, *et al*: Revealing and harnessing CD39 for the treatment of colorectal cancer and liver metastases by engineered T cells. Gut 72: 1887-1903, 2023.
34. Khaliq AM, Erdogan C, Kurt Z, Turgut SS, Grunvald MW, Rand T, Khare S, Borgia JA, Hayden DM, Pappas SG, *et al*: Refining colorectal cancer classification and clinical stratification through a single-cell atlas. Genome Biol 23: 113, 2022.
35. Love MI, Huber W and Anders S: Moderated estimation of fold change and dispersion for RNA-seq data with DESeq2. Genome Biol 15: 550, 2014.
36. Langfelder P and Horvath S: WGCNA: An R package for weighted correlation network analysis. BMC Bioinformatics 9: 559, 2008.
37. Sun X, Deng Q, Liang Z, Liu Z, Geng H, Zhao L, Zhou Q, Liu J, Ma J, Wang D, *et al*: Cigarette smoke extract induces epithelial-mesenchymal transition of human bladder cancer T24 cells through activation of ERK1/2 pathway. Biomed Pharmacother 86: 457-465, 2017.
38. Liang Z, Lu L, Mao J, Li X, Qian H and Xu W: Curcumin reversed chronic tobacco smoke exposure induced urocystic EMT and acquisition of cancer stem cells properties via Wnt/β-catenin. Cell Death Dis 8: e3066, 2017.
39. Qian Y, Liu Z, Liu Q, Tian X, Mo J, Leng L, Wang C, Xu G, Zhang S and Xie J: Transduction of lentiviral vectors and ADORA3 in HEK293T cells modulated in gene expression and alternative splicing. Int J Mol Sci 26: 4431, 2025.
40. Escrivá-Fernández J, Cueto-Ureña C, Solana-Orts A, Lledó E, Ballester-Lurbe B and Poch E: A CRISPR interference strategy for gene expression silencing in multiple myeloma cell lines. J Biol Eng 17: 34, 2023.
41. Elegheert J, Behiels E, Bishop B, Scott S, Woolley RE, Griffiths SC, Byrne EFX, Chang VT, Stuart DI, Jones EY, *et al*: Lentiviral transduction of mammalian cells for fast, scalable and high-level production of soluble and membrane proteins. Nat Protoc 13: 2991-3017, 2018.
42. Livak KJ and Schmittgen TD: Analysis of relative gene expression data using real-time quantitative PCR and the 2(-Delta Delta C(T)) method. Methods 25: 402-408, 2001.
43. Mei S, Qin Q, Wu Q, Sun H, Zheng R, Zang C, Zhu M, Wu J, Shi X, Taing L, *et al*: Cistrome data browser: A data portal for ChIP-Seq and chromatin accessibility data in human and mouse. Nucleic Acids Res 45 (D1): D658-D662, 2017.
44. Rauluseviciute I, Riudavets-Puig R, Blanc-Mathieu R, Castro-Mondragon JA, Ferenc K, Kumar V, Lemma RB, Lucas J, Chèneby J, Baranasic D, *et al*: JASPAR 2024: 20th anniversary of the open-access database of transcription factor binding profiles. Nucleic Acids Res 52 (D1): D174-D182, 2024.
45. Nakanishi T, Koma YI, Miyako S, Torigoe R, Yokoo H, Omori M, Yamanaka K, Ishihara N, Tsukamoto S, Kodama T, *et al*: AREG upregulation in cancer cells via direct interaction with cancer-associated fibroblasts promotes esophageal squamous cell carcinoma progression through EGFR-Erk/p38 MAPK signaling. Cells 13: 1733, 2024.
46. Keum N and Giovannucci E: Global burden of colorectal cancer: Emerging trends, risk factors and prevention strategies. Nat Rev Gastroenterol Hepatol 16: 713-732, 2019.
47. Roshandel G, Ghasemi-Kebria F and Malekzadeh R: Colorectal cancer: Epidemiology, risk factors, and prevention. Cancers (Basel) 16: 1530, 2024.
48. Gausman V, Dornblaser D, Anand S, Hayes RB, O'Connell K, Du M and Liang PS: Risk factors associated with early-onset colorectal cancer. Clin Gastroenterol Hepatol 18: 2752-2759.e2, 2020.
49. Islami F, Marlow EC, Thomson B, McCullough ML, Rumgay H, Gapstur SM, Patel AV, Soerjomataram I and Jemal A: Proportion and number of cancer cases and deaths attributable to potentially modifiable risk factors in the United States, 2019. CA Cancer J Clin 74: 405-432, 2024.
50. Li K, Zhang R, Zhang J, Zhang Z, Wang K, Lu Y, Zhao Z, Chen Y and Ma S: The prognostic role of inflammation-based hematologic markers in stage I-III colorectal cancer: A retrospective analysis. BMC Cancer 25: 1822, 2025.
51. Ugai T, Väyrynen JP, Haruki K, Akimoto N, Lau MC, Zhong R, Kishikawa J, Väyrynen SA, Zhao M, Fujiyoshi K, *et al*: Smoking and incidence of colorectal cancer subclassified by tumor-associated macrophage infiltrates. J Natl Cancer Inst 114: 68-77, 2022.
52. Hamada T, Nowak JA, Masugi Y, Drew DA, Song M, Cao Y, Kosumi K, Mima K, Twombly TS, Liu L, *et al*: Smoking and risk of colorectal cancer sub-classified by tumor-infiltrating T cells. J Natl Cancer Inst 111: 42-51, 2019.
53. Botteri E, Borroni E, Sloan EK, Bagnardi V, Bosetti C, Peveri G, Santucci C, Specchia C, van den Brandt P, Gallus S and Lugo A: Smoking and colorectal cancer risk, overall and by molecular subtypes: A meta-analysis. Am J Gastroenterol 115: 1940-1949, 2020.
54. Flor LS, Anderson JA, Ahmad N, Aravkin A, Carr S, Dai X, Gil GF, Hay SI, Malloy MJ, McLaughlin SA, *et al*: Health effects associated with exposure to secondhand smoke: A burden of proof study. Nat Med 30: 149-167, 2024.
55. Dimou N, Yarmolinsky J, Bouras E, Tsilidis KK, Martin RM, Lewis SJ, Gram IT, Bakker MF, Brenner H, Figueiredo JC, *et al*: Causal effects of lifetime smoking on breast and colorectal cancer risk: Mendelian randomization study. Cancer Epidemiol Biomarkers Prev 30: 953-964, 2021.
56. Ferraro M, Di Vincenzo S, Lazzara V, Pinto P, Patella B, Inguanta R, Bruno A and Pace E: Formoterol exerts anti-cancer effects modulating oxidative stress and epithelial-mesenchymal transition processes in cigarette smoke extract exposed lung adenocarcinoma cells. Int J Mol Sci 24: 16088, 2023.
57. Yumoto T, Nakadate K, Nakamura Y, Sugitani Y, Sugitani-Yoshida R, Ueda S and Sakakibara S: Radmis, a novel mitotic spindle protein that functions in cell division of neural progenitors. PLoS One 8: e79895, 2013.
58. Liu Y, Chen Y, Wang F, Lin J, Tan X, Chen C, Wu LL, Zhang X, Wang Y, Shi Y, *et al*: Caveolin-1 promotes glioma progression and maintains its mitochondrial inhibition resistance. Discov Oncol 14: 161, 2023.
59. Zhang Y, Luo J, Liu Z, Liu X, Ma Y, Zhang B, Chen Y, Li X, Feng Z, Yang N, *et al*: Identification of hub genes in colorectal cancer based on weighted gene co-expression network analysis and clinical data from the cancer genome atlas. Biosci Rep 41: BSR20211280, 2021.
60. Liu Z, Zhang J, Shen D, Hu X, Ke Z, Ehrich Lister IN and Sihombing B: Prognostic significance of CKAP2L expression in patients with clear cell renal cell carcinoma. Front Genet 13: 873884, 2023.
61. Xiong G, Li L, Chen X, Song S, Zhao Y, Cai W and Peng J: Up-regulation of CKAP2L expression promotes lung adenocarcinoma invasion and is associated with poor prognosis. Onco Targets Ther 12: 1171-1180, 2019.
62. Li Q, Yan M, Wang C, Wang K and Bao G: CKAP2L, a crucial target of miR-326, promotes prostate cancer progression. BMC Cancer 22: 666, 2022.
63. Yi B, Fu Q, Zheng Z, Zhang M, Liu D, Liang Z, Xu S and Zhang Z: Pan-cancer analysis reveals the prognostic and immunotherapeutic value of cytoskeleton-associated protein 2-like. Sci Rep 13: 8368, 2023.
64. Chi F, Chen L, Jin X, He G, Liu Z and Han S: CKAP2L, transcriptionally inhibited by FOXP3, promotes breast carcinogenesis through the AKT/mTOR pathway. Exp Cell Res 412: 113035, 2022.
65. Berasain C and Avila MA: Amphiregulin. Semin Cell Dev Biol 28: 31-41, 2014.

66. Napolitano S, Martini G, Ciardiello D, Del Tufo S, Martinelli E, Troiani T and Ciardiello F: Targeting the EGFR signalling pathway in metastatic colorectal cancer. Lancet Gastroenterol Hepatol 9: 664-676, 2024.
67. Zhang W, Zhang W, Tang C, Hu Y, Yi K, Xu X and Chen Z: Silencing AREG enhances sensitivity to irradiation by suppressing the PI3K/AKT signaling pathway in colorectal cancer cells. Biologics 18: 273-284, 2024.
68. Sun R, Zhao H, Gao DS, Ni A, Li H, Chen L, Lu X, Chen K and Lu B: Amphiregulin couples IL1RL1^{+} regulatory T cells and cancer-associated fibroblasts to impede antitumor immunity. Sci Adv 9: eadd7399, 2023.
69. Hu Y, Dong Z and Liu K: Unraveling the complexity of STAT3 in cancer: Molecular understanding and drug discovery. J Exp Clin Cancer Res 43: 23, 2024.
70. Zou S, Tong Q, Liu B, Huang W, Tian Y and Fu X: Targeting STAT3 in cancer immunotherapy. Mol Cancer 19: 145, 2020.
71. Samad MA, Ahmad I, Hasan A, Alhashmi MH, Ayub A, Al-Abbasi FA, Kumer A and Tabrez S: STAT3 signaling pathway in health and disease. MedComm (2020) 6: e70152, 2025.
72. Pennel KAF, Hatthakarnkul P, Wood CS, Lian GY, Al-Badran SSF, Quinn JA, Legrini A, Inthagard J, Alexander PG, van Wyk H, *et al*: JAK/STAT3 represents a therapeutic target for colorectal cancer patients with stromal-rich tumors. J Exp Clin Cancer Res 43: 64, 2024.